^{18}F-Labeled Bombesin Analogs for Targeting GRP Receptor-Expressing Prostate Cancer

Xianzhong Zhang, PhD[1]; Weibo Cai, PhD[1]; Feng Cao, MD, PhD[1]; Eduard Schreibmann, PhD[2]; Yun Wu, PhD[1]; Joseph C. Wu, MD, PhD[1,3]; Lei Xing, PhD[2]; and Xiaoyuan Chen, PhD[1]

[1]Molecular Imaging Program at Stanford (MIPS), Department of Radiology and Bio-X Program, Stanford University School of Medicine, Stanford, California; [2]Department of Radiation Oncology, Stanford University School of Medicine, Stanford, California; and [3]Division of Cardiology, Department of Medicine, Stanford University School of Medicine, Stanford, California

The gastrin-releasing peptide receptor (GRPR) is found to be overexpressed in a variety of human tumors. The aim of this study was to develop ^{18}F-labeled bombesin analogs for PET of GRPR expression in prostate cancer xenograft models. **Methods:** [Lys^3]Bombesin ([Lys^3]BBN) and aminocaproic acid-bombesin(7–14) (Aca-BBN(7–14)) were labeled with ^{18}F by coupling the Lys^3 amino group and Aca amino group, respectively, with *N*-succinimidyl-4-^{18}F-fluorobenzoate (^{18}F-SFB) under slightly basic condition (pH 8.5). Receptor-binding affinity of FB-[Lys^3]BBN and FB-Aca-BBN(7–14) was tested in PC-3 human prostate carcinoma cells. Internalization and efflux of both radiotracers were also evaluated. Tumor-targeting efficacy and in vivo kinetics of both radiotracers were examined in male athymic nude mice bearing subcutaneous PC-3 tumors by means of biodistribution and dynamic microPET imaging studies. ^{18}F-FB-[Lys^3]BBN was also tested for orthotopic PC-3 tumor delineation. Metabolic stability of ^{18}F-FB-[Lys^3]BBN was determined in mouse blood, urine, liver, kidney, and tumor homogenates at 1 h after injection. **Results:** The typical decay-corrected radiochemical yield was about 30%–40% for both tracers, with a total reaction time of 150 ± 20 min starting from ^{18}F$^-$. ^{18}F-FB-[Lys^3]BBN had moderate stability in the blood and PC-3 tumor, whereas it was degraded rapidly in the liver, kidneys, and urine. Both radiotracers exhibited rapid blood clearance. ^{18}F-FB-[Lys^3]BBN had predominant renal excretion. ^{18}F-FB-Aca-BBN(7–14) exhibited both hepatobiliary and renal clearance. Dynamic microPET imaging studies revealed that the PC-3 tumor uptake of ^{18}F-FB-[Lys^3]BBN in PC-3 tumor was much higher than that of ^{18}F-FB-Aca-BBN(7–14) at all time points examined ($P < 0.01$). The receptor specificity of ^{18}F-FB-[Lys^3]BBN in vivo was demonstrated by effective blocking of tumor uptake in the presence of [Tyr^4]BBN. No obvious blockade was found in PC-3 tumor when ^{18}F-FB-Aca-BBN(7–14) was used as radiotracer under the same condition. ^{18}F-FB-[Lys^3]BBN was also able to visualize orthotopic PC-3 tumor at early time points after tracer administration, at which time minimal urinary bladder activity was present to interfere with the receptor-mediated tumor uptake. **Conclusion:** This study demonstrates that ^{18}F-FB-[Lys^3]BBN and PET are suitable for detecting GRPR-positive prostate cancer in vivo.

Key Words: prostate cancer; GRP receptor; ^{18}F-bombesin; microPET; microCT

J Nucl Med 2006; 47:492–501

Neuroendocrine (NE) cells are believed to play a paracrine regulatory role in the prostate (*1*). Prostatic NE cells contain abundant secretory granules filled with numerous bioactive compounds collectively called NE products (NEP) (*2*). In particular, members of the gastrin-releasing peptide (GRP) family and its analog bombesin (BBN) have been implicated in the biology of several human malignancies, including lung, colon, breast, and prostate cancers (*1–4*). To date, 3 mammalian GRP/BBN receptor subtypes have been cloned and characterized: the GRP receptor (GRPR), the BBN-receptor subtype 3 (BRS-3), and the neuromedin-B receptor (NMBR) (*5*). Only GRPR was found in prostate carcinoma (*6*), although NMBR and BSR-3 have been found in other cancer types (*7,8*). Antagonists of GRPR are designed to bind to human GRPR with high affinity and block the receptor-activated signal transduction pathways and, thus, inhibit the growth of prostate cancer both in vitro and in vivo (*9*). GRP/BBN analogs have also been used as carriers to deliver drugs, radionuclides, and toxins to target prostate carcinoma and other cancer types that are GRPR positive (*10,11*). Therefore, the ability to document GRPR density in vivo is crucial for the application of GRPR-targeted drug delivery.

Being the most widely applied radionuclide for diagnostic purposes, a great deal of research has been done to develop ^{99m}Tc- and ^{111}In-labeled BBN-like peptides involving a wide range of chelators, peptide sequences, and bifunctional linkers (*12*). To date, 2 of the de novo radiolabeled GRP-like peptides, RP527 (*13*) and the BN1 (*14*), are under clinical evaluation with satisfactory results. In addition, ^{90}Y, ^{188}Re, and ^{177}Lu have been used to radiolabel BBN analogs for potential peptide receptor radiotherapy applications (*15,16*).

PET for cancer imaging of GRPR status in vivo has been less studied. Rogers et al. developed a truncated form of a

---

Received Sep. 28, 2005; revision accepted Nov. 15, 2005.

For correspondence or reprints contact: Xiaoyuan Chen, PhD, Molecular Imaging Program at Stanford (MIPS), Department of Radiology and Bio-X Program, Stanford University School of Medicine, 1201 Welch Rd., P095, Stanford, CA 94305-5484.

E-mail: shawchen@stanford.edu

^{64}Cu (half-life [$t_{1/2}$] = 12.7 h; β^+, 17.4%)-labeled BBN analog, ^{64}Cu-DOTA-Aoc-BBN(7–14) (Aoc is 8-aminooctanoic acid), for microPET imaging of an androgen-independent PC-3 tumor xenograft model (*17*). Incorporation of a poly(ethylene glycol) (PEG) linker (molecular weight 3,400) resulted in significantly reduced receptor avidity and lower receptor specific activity accumulation in vivo (*18*). We recently reported the synthesis and pharmacologic evaluation of another ^{64}Cu-labeled BBN analog, ^{64}Cu-DOTA-[Lys^3]BBN, for targeting GRPR expression in both PC-3 and 22RV1 tumor models (*19*). Very recently, another BBN analog, [D-Tyr^6,β-Ala^{11}, Thi^{13},Nle^{14}]BBN(6–14) amide (BZH3), was conjugated with 1,4,7,10-tetraazacyclododecane-*N,N′,N′′,N′′′*-tetraacetic acid (DOTA) through a PEG2 linker and labeled with ^{68}Ga ($t_{1/2}$ = 68 min; β^+, 88%), obtained from a ^{68}Ge/^{68}Ga generator for imaging AR42J rat pancreatic cancer-bearing nude mice (*20*).

^{18}F ($t_{1/2}$ = 109.7 min; β^+, 99%) is an ideal short-lived PET isotope for labeling small molecular recognition units such as antigen- binding domain of antibody fragments and small biologically active peptides (*21*). ^{18}F-Labeled prosthetic groups such as *N*-succinimidyl-4-^{18}F-fluorobenzoate (^{18}F-SFB) have been developed, which can be attached to either N-terminal or lysine ε-amino groups with little or no loss of bioactivity of the peptide ligand (*22,23*). In the present study, we labeled both [Lys^3]bombesin ([Lys^3]BBN) and aminocaproic acid-bombesin(7–14) (Aca-BBN(7–14)) with ^{18}F for GRPR imaging of subcutaneous and orthotopic PC-3 tumor models with PET.

MATERIALS AND METHODS

Materials

All chemicals obtained commercially were used without further purification. [Lys^3]BBN and Aca-BBN(7–14) were synthesized using solid-phase Fmoc chemistry by American Peptide, Inc. No-carrier-added ^{18}F$^-$ was obtained from PETNET Inc. The received ^{18}F$^-$ was trapped on an anion-exchange resin and eluted with 0.5 mL K_2CO_3 (2 mg/mL in H_2O) combined with 1 mL Kryptofix 2.2.2. (Sigma-Aldrich) (10 mg/mL in acetonitrile). The semipreparative reversed-phase high-performance liquid chromatography (HPLC) system has been described elsewhere (*24*).

Chemistry and Radiochemistry

4-Fluorobenzoyl-bombesin analogs (FB-[Lys^3]BBN and FB-Aca-BBN(7–14)) were synthesized as reference standards. In brief, an equimolar amount of SFB (in acetonitrile) and [Lys^3]BBN or Aca-BBN(7–14) (in H_2O) was mixed and the pH was adjusted to 8.3 by addition of 0.1N sodium borate buffer. The reaction mixture was incubated at 40°C for 80 min and then quenched by trifluoroacetic acid (TFA). Semipreparative HPLC purification gave the desired products. The HPLC retention times were around 20.8 min for FB-[Lys^3]BBN and 19.1 min for FB-Aca-BBN(7–14), respectively.

4-^{18}F-Fluorobenzoyl-[Lys^3]bombesin (^{18}F-FB-[Lys^3]BBN) and 4-^{18}F-fluorobenzoyl-Aca-bombesin(7–14) (^{18}F-FB-Aca-BBN(7–14)) were synthesized by coupling the corresponding BBN peptide with ^{18}F-SFB (*25–27*). ^{18}F-SFB was purified by semipreparative HPLC, concentrated to about 200 μL, and added to [Lys^3]BBN or Aca-BBN(7–14) peptide (200 μg) in 800 μL of sodium borate buffer (50 mmol/L, pH 8.5). The reaction mixture was gently mixed at 40°C for 30 min. Final purification was accomplished by semipreparative HPLC and the tracers were reconstituted in phosphate-buffered saline (PBS, pH 7.4) and passed through a 0.22-μm Millipore filter (Millipore Corp.) for in vivo applications.

In Vitro Cell-Binding Assay

The PC-3 human prostate carcinoma cell line was purchased from American Type Culture Collection. PC-3 cells were grown in F-12K nutrient mixture (Kaighn's modification) (Invitrogen Corp.) supplemented with 10% (v/v) fetal bovine serum (FBS) (Invitrogen Corp.) at 37°C with 5% CO_2. In vitro binding affinity and specificity of FB-BBN analogs for GRPR were evaluated using competitive receptor-binding assay. ^{125}I-[Tyr^4]BBN (Perkin-Elmer Life Science Products, Inc.; specific activity, 74 TBq/mmol) was used as the GRPR-specific radioligand. Experiments were performed as described previously (*19*). The 50% inhibitory concentration (IC_{50}) value for the displacement binding of ^{125}I-[Tyr^4]BBN by those ligands was calculated by nonlinear regression analysis using GraphPad Prism software (Graph-Pad Software Inc.). All experiments were performed twice with triplicate samples.

Internalization and Efflux Studies

Internalization and efflux of ^{18}F-FB-[Lys^3]BBN and ^{18}F-FB-Aca-BBN(7–14) into PC-3 cells were examined following a protocol reported earlier (*19*). The data was normalized as percentage of the total amount of radioactivity added per cell.

Animal Models

All animal experiments were performed under a protocol approved by the Stanford University Administrative Panel on Laboratory Animal Care (A-PLAC). Both subcutaneous and orthotopic tumor model were established in 4- to 6-wk-old male athymic *nu/nu* mice (Harlan). For the subcutaneous prostate cancer model, 5×10^6 PC-3 cells suspended in 50 μL serum-free F-12K medium and 50 μL Matrigel (BD Biosciences) were injected into the right shoulder of the mice. For the orthotopic PC-3 tumor model, 5×10^5 cells in 20 μL PBS were injected into the prostate gland of male nude mice. The prostate of anesthetized mice was exposed through a midline laparotomy incision and by retraction of the bladder and male sex accessory glands anteriorly. Injection of cells was performed with a 27-gauge needle inserted into the prostatic lobe located at the base of the seminal vesicles as described (*28*). The abdominal wound was sutured using a 4.0 chromic gut suture in a running fashion.

Biodistribution

The subcutaneous tumor-bearing mice were used for biodistribution when the tumor volume reached 300–400 mm^3 (3–4 wk after inoculation). Three mice were each injected intravenously with about 370 kBq (10 μCi) ^{18}F-FB-[Lys^3]BBN or ^{18}F-FB-Aca-BBN(7–14). The mice were sacrificed at 60 min after injection and the body weight was recorded. Blood, tumor, major organs, and tissues were collected, wet weighed, and counted by γ-counter. The percentage of injected dose per gram (%ID/g) was determined for each sample. For each mouse, radioactivity of the tissue samples was calibrated against a known aliquot of radiotracer. Values are expressed as mean ± SD. To test the specific binding of the radiotracers to PC-3 tumor, GRPR-blocking studies were performed by examining the biodistribution of each radiolabeled tracer in the presence of [Try^4]BBN as a blocking agent

(10 mg/kg mice body weight). Mice were also sacrificed at 60 min after injection ($n = 3$).

microPET Imaging and Image Analysis

microPET scans were performed on a microPET R4 rodent model scanner (Concorde Microsystems Inc.). The scanner has a computer-controlled bed and 10.8-cm transaxial and 8-cm axial fields of view (FOVs). It has no septa and operates exclusively in the 3-dimensional (3D) list mode. Animals were placed near the center of the FOV of the scanner, where the highest image resolution and sensitivity are available. The microPET studies were performed by tail-vein injection of 3.7 MBq (100 μCi) of radiotracer (^{18}F-FB-[Lys^3]BBN or ^{18}F-FB-Aca-BBN(7–14)) under isoflurane anesthesia. The 60-min dynamic (5 × 1 min, 5 × 2 min, 5 × 3 min, 6 × 5 min) microPET data acquisition (total of 21 frames) was started 4 min after injection. Static images at 2.5-, 3-, and 4-h time points were also acquired as 10-min static images. The images were reconstructed by a 2-dimensional ordered-subsets expectation maximum (OSEM) algorithm and no correction was necessary for attenuation or scatter (*29*).

For each microPET scan, regions of interest (ROIs) were drawn over the tumor, normal tissue, and major organs by using vendor software (ASI Pro 5.2.4.0) on decay-corrected whole-body coronal images. The maximum radioactivity concentration (accumulation) within a tumor or an organ was obtained from mean pixel values within the multiple ROI volume, which were converted to counts/mL/min by using a conversion factor. Assuming a tissue density of 1 g/mL, the ROIs were converted to counts/g/min and then divided by the administered activity to obtain an imaging ROI–derived %ID/g.

Metabolic Stability

Male mice bearing PC-3 tumors were injected intravenously with 3.7 MBq of ^{18}F-FB-[Lys^3]BBN. The animals were sacrificed and dissected at 60 min after injection Blood, urine, liver, kidneys, and tumor were collected. Blood was immediately centrifuged for 5 min at 13,200 rpm. Organs were homogenized using an IKA Ultra-Turrax T8 (IKA Works Inc.), suspended in 1 mL of PBS, and centrifuged for 5 min at 13,200 rpm. After removal of the supernatants, the pellets were washed with 500 μL of PBS. For each sample, supernatants of both centrifugation steps were combined and passed through Sep-Pak C_{18} cartridges. The urine sample was directly diluted with 1 mL of PBS and passed through Sep-Pak C_{18} cartridge. The cartridges were washed with 2 mL of H_2O and eluted with 2 mL of acetonitrile containing 0.1% TFA. The combined aqueous and organic solutions were concentrated to about 1 mL by rotary evaporation, passed through a 0.22-μm Millipore filter, and injected onto an analytic HPLC column at a flow rate of 1 mL/min using the gradient described earlier. Radioactivity was monitored using a solid-state radiation detector. At the same time, the eluent was also collected by a fraction collector (0.5 min/fraction), and the activity of each fraction was measured by the γ-counter. The HPLC analysis was performed in duplicate and the extraction efficiency was determined in triplicate. Data obtained from the γ-counter were plotted to reconstruct the HPLC chromatograms. Control experiments were also performed to test the extraction and elution efficiency by adding ^{18}F-FB-[Lys^3]BBN directly to the same tissue samples.

microCT Imaging

To perform a microCT scan, an anesthetized male nude mouse bearing an orthotopic PC-3 tumor (4–6 wk after inoculation) was mounted on a turntable bed that could be moved automatically in the axial direction. The high-resolution 3D images were obtained by a commercial microCAT II system (ImTek Inc.). This scanner uses a SourceRay SB-80-50 x-ray tube with about 40-μm focal spot providing 30-μm resolution in high-resolution configuration. A total of 220 rotation steps was taken over 220° with one axial bed position. A standard convolution-backprojection procedure with a Shepp–Logan filter was used to reconstruct the CT images in 512 × 512 pixel matrices.

microPET and microCT Image Fusion

For the microPET and microCT coregistration, we used a narrow-band approach, which is a hybrid method combining the advantages of pixel-based and distance-based registration techniques (*30*). In essence, this technique is a 2-step image registration in which the tumor to be registered is first represented by a data structure containing the signed distance values from its boundaries, followed by an image registration using a pixel-based metric. The optimization aligns the zero set of the narrow band obtained from the CT images with the tumor gradients in the PET dataset, eliminating the assumption of uniform pixel intensities within one organ used in the mutual information (MI) approach. In our setup, the normalized correlation was used as the metric and a gradient-based algorithm was used to find the optimal match.

Histology

After imaging, both subcutaneous and orthotopic tumors were dissected for histology to verify tumor pathology. Tumor tissues were frozen at −80°C in optimal cutting temperature (OCT) medium. Frozen sections (5 μm; Leica Microsystems, Inc.) were fixed in acetone at −20°C for 15 min and air-dried overnight (4°C). They were then stained with hematoxylin–eosin (BD Biosciences). Slides were examined under a ZEISS AxioVert 25 research microscope (Carl Zeiss) equipped with a ZEISS digital camera (model AxioCam MRc5) and captured with MRGrab 1.0.0.4 (Carl Zeiss vision GmbH) software.

Statistical Analysis

Quantitative data are expressed as mean ± SD. Means were compared using 1-way ANOVA and the Student *t* test. P values $<$ 0.05 were considered significant.

RESULTS

Radiosynthesis

^{18}F-Fluorination of bombesin analogs ([Lys^3]BBN and Aca-BBN(7–14)) were achieved via ^{18}F-SFB (Fig. 1). Starting with ^{18}F-F$^-$ in Kryptofix 2.2.2./K_2CO_3 solution, the total reaction time, including final HPLC purification, was about 150 ± 20 min. The overall radiochemical yield with decay correction was 31.4% ± 4.6% ($n = 12$). The radiochemical purity of the labeled peptides was >98% according to analytic HPLC. The specific activity of ^{18}F-SFB was estimated by radio-HPLC to be 200−250 TBq/mmol. ^{18}F-FB-[Lys^3]BBN and ^{18}F-FB-Aca-BBN(7–14) were well separated from [Lys^3]BBN and Aca-BBN(7–14), respectively, rendering the specific activity of these 2 PET tracers virtually the same as that of ^{18}F-SFB.

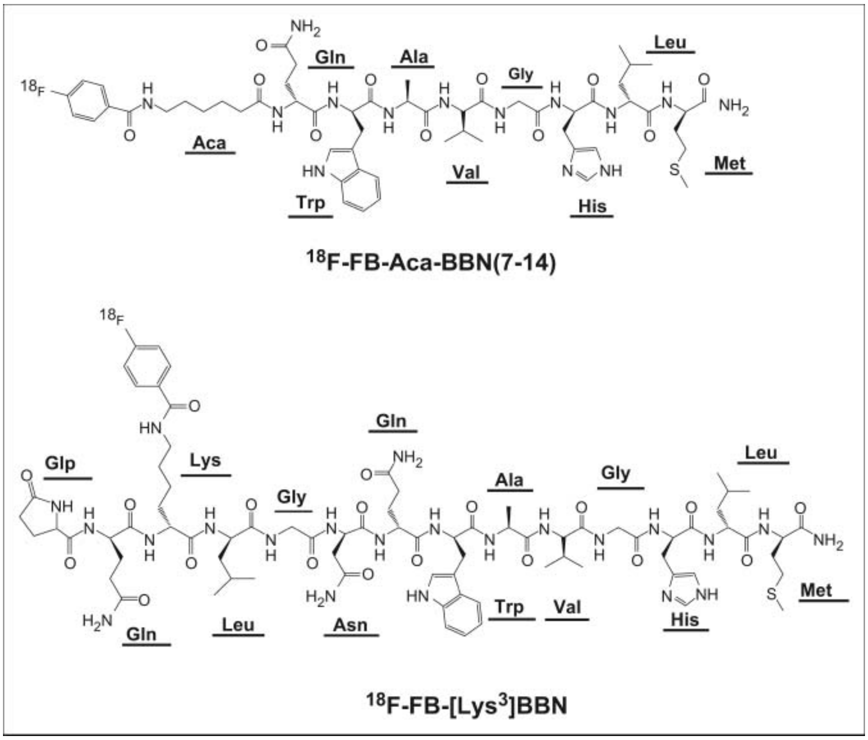

FIGURE 1. Schematic structures of ^{18}F-FB-Aca-BBN(7–14) and ^{18}F-FB-[Lys^3]BBN.

In Vitro Receptor-Binding Assay

The binding affinities of [Lys^3]BBN, Aca-BBN(7–14), FB-[Lys^3]BBN, and FB-Aca-BBN(7–14) for GRPR were evaluated for PC-3 cells. Results of the cell-binding assay were plotted in sigmoid curves for the displacement of ^{125}I-[Tyr^4]BBN from PC-3 cells as a function of increasing concentration of bombesin analogs. The IC$_{50}$ values were determined to be 3.3 ± 0.4 nmol/L for [Lys^3]BBN, 20.8 ± 0.3 nmol/L for Aca-BBN(7–14), 5.3 ± 0.6 nmol/L for FB-[Lys^3]BBN, and 48.7 ± 0.1 nmol/L for FB-Aca-BBN(7–14) on 1×10^5 PC-3 cells. [Lys^3]BBN with the full sequence of the bombesin peptide is substantially more potent than Aca-BBN(7–14) with the truncated sequence. Coupling of the fluorobenzoyl group had a minimal effect on the binding affinity for both compounds.

Internalization and Efflux Studies

The results for the internalization of both tracers, ^{18}F-FB-[Lys^3]BBN and ^{18}F-FB-Aca-BBN(7–14), are shown in Figure 2A. For both tracers, internalization occurred during 5 min of incubation after the preincubation step: 51% for ^{18}F-FB-[Lys^3]BBN and 58% for ^{18}F-FB-Aca-BBN(7–14), respectively. After approximately 15 min of incubation, internalization of both tracers reached a maximum (85% for ^{18}F-FB-[Lys^3]BBN and 60% for ^{18}F-FB-Aca-BBN(7–14)) and then decreased slowly through 120 min of incubation (61% for ^{18}F-FB-[Lys^3]BBN and 50% for ^{18}F-FB-Aca-BBN(7–14) at 120 min). When blocked with 200 μmol/L of [Tyr^4]BBN, the nonspecific uptake for both tracers was <10% over the incubation period (data not shown).

Efflux studies were performed for up to 3 h of incubation to further characterize both tracers (Fig. 2B). ^{18}F-FB-[Lys^3]BBN and ^{18}F-FB-Aca-BBN(7–14) tracers exhibited similar efflux curves. After 30 min of incubation, approximately 54% of ^{18}F-FB-[Lys^3]BBN had effluxed out of the cells. At the end of the 3-h incubation period, approximately 77% of the radiotracer had effluxed. For ^{18}F-FB-Aca-BBN(7–14) tracer, after 30 min of incubation, approximately 39% of the radioactivity effluxed out of the PC-3 cells and, after 3 h of incubation, approximately 83% of the radioactivity had effluxed. The efflux rate of ^{18}F-FB-Aca-BBN(7–14) is faster than that of ^{18}F-FB-[Lys^3]BBN, which might be due to the lower affinity of ^{18}F-FB-Aca-BBN(7–14) for the GRPR than ^{18}F-FB-[Lys^3]BBN, as determined from the in vitro cell-binding assay.

Biodistribution

Biodistribution of ^{18}F-FB-[Lys^3]BBN and ^{18}F-FB-Aca-BBN(7–14) was evaluated in athymic nude mice bearing subcutaneous PC-3 tumors. The results were shown in Figure 3. For ^{18}F-FB-[Lys^3]BBN (Fig. 3A), the tumor uptake was 5.94 ± 0.78 %ID/g at 60 min after injection, which decreased to 0.50 ± 0.11 %ID/g in the presence of a blocking dose of [Tyr^4]BBN (10 mg/kg mice body weight). [Tyr^4]BBN was also able to substantially reduce the activity accumulation in the pancreas, intestines, and kidneys, demonstrating that these organs are also GRPR positive. Increased uptake in the lung, liver, and spleen was observed. For ^{18}F-FB-Aca-BBN(7–14) (Fig. 3B), the tumor uptake (0.43 ± 0.18 %ID/g at 60 min after injection) was more than one order of magnitude lower than that for

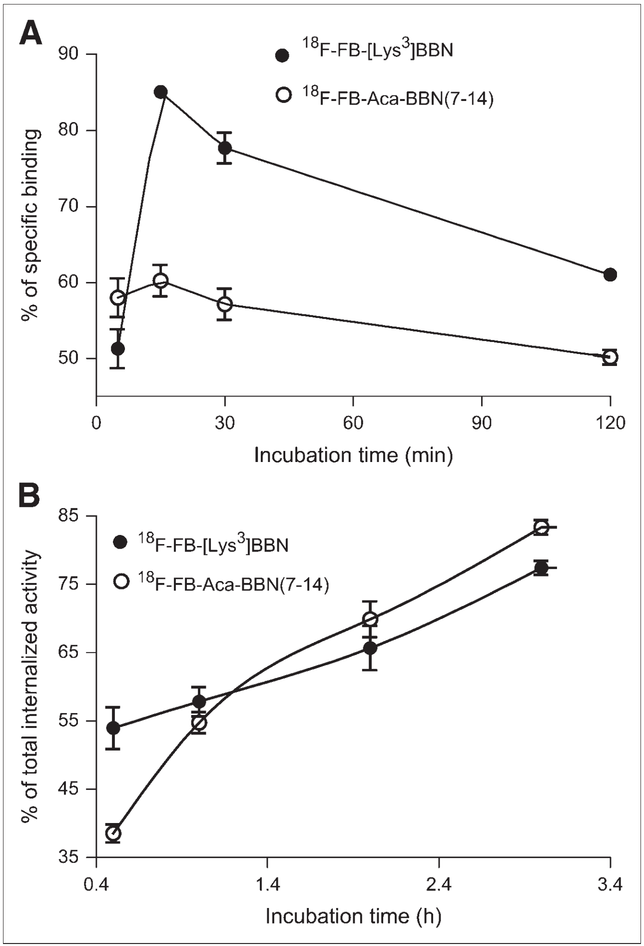

FIGURE 2. Comparison of internalization (A) and efflux rate (B) of ^{18}F-FB-[Lys^3]BBN and ^{18}F-FB-Aca-BBN(7–14) using PC-3 cells. Data are from 2 experiments with triplicate samples and are expressed as mean ± SD.

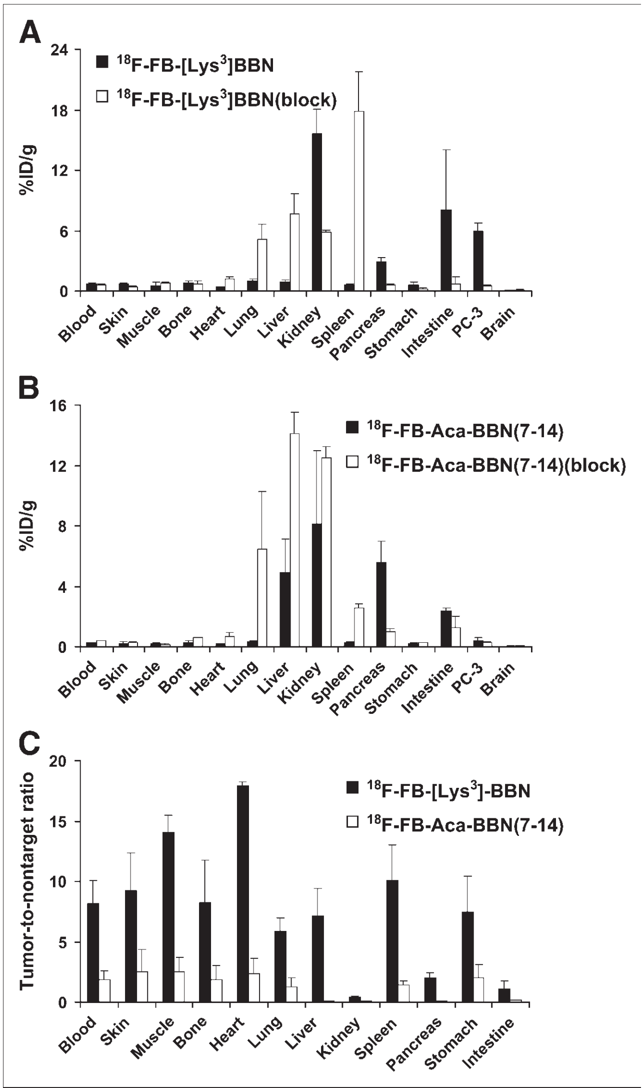

FIGURE 3. Biodistribution of ^{18}F-FB-[Lys^3]BBN (A) and ^{18}F-FB-Aca-BBN(7–14) (B) in male athymic nude mice bearing subcutaneous PC-3 tumors. Mice were injected intravenously with 370 kBq of radioligand with or without the presence of [Tyr^4]BBN at 10 mg/kg mice body weight and euthanized at 60 min after injection. (C) Tumor-to-nontarget ratios of 2 radiotracers resulting from the biodistribution are also shown. Data are presented as mean %ID/g ± SD ($n = 3$).

^{18}F-FB-[Lys^3]BBN. A blocking dose of [Tyr^4]BBN decreased the uptake of ^{18}F-FB-Aca-BBN(7–14) in the tumor, pancreas, and intestines, whereas the uptake in the liver, kidneys, and lung was increased. Tumor-to-nontarget ratios of ^{18}F-FB-[Lys^3]BBN were significantly higher than those of ^{18}F-FB-Aca-BBN(7–14) for all organs and tissues examined ($P < 0.001$) (Fig. 3C).

Dynamic microPET Imaging of Subcutaneous PC-3 Tumor Model

The dynamic microPET scans were performed on the subcutaneous PC-3 tumor model with ^{18}F-FB-[Lys^3]BBN and ^{18}F-FB-Aca-BBN(7–14). Selected coronal images at different time points after administration of the appropriate tracers are shown in Figure 4 for comparison. Tumor contrast was observed as early as 10 min after injection for both radiotracers. The tumor uptake of ^{18}F-FB-[Lys^3]BBN was 3.50, 3.68, and 2.61 %ID/g at 10, 30, and 60 min after injection, respectively. The tumor-to-contralateral background (muscle) ratio was 3.95 at 60 min after injection Time–activity curves derived from the 60-min dynamic microPET scan showed that ^{18}F-FB-[Lys^3]BBN was excreted predominantly through the renal route (Fig. 5A). Liver had low initial uptake (5.15 %ID/g at 5 min after injection) and the radioactivity was also washed out rapidly (1.75 %ID/g at 1 h after injection). The activity accumulation in the kidneys was moderately low at early time points (4.85 %ID/g at 5 min after injection) but rapidly increased to 47.00 %ID/g at 50 min after injection followed by a steep decline afterward (28.49 %ID/g at 60 min and 1.01 %ID/g at 2 h after injection). Compared with ^{18}F-FB-[Lys^3]BBN, ^{18}F-FB-Aca-BBN(7–14) had a significantly lower tumor uptake, which corroborates the biodistribution results obtained from direct tissue sampling. The tumor

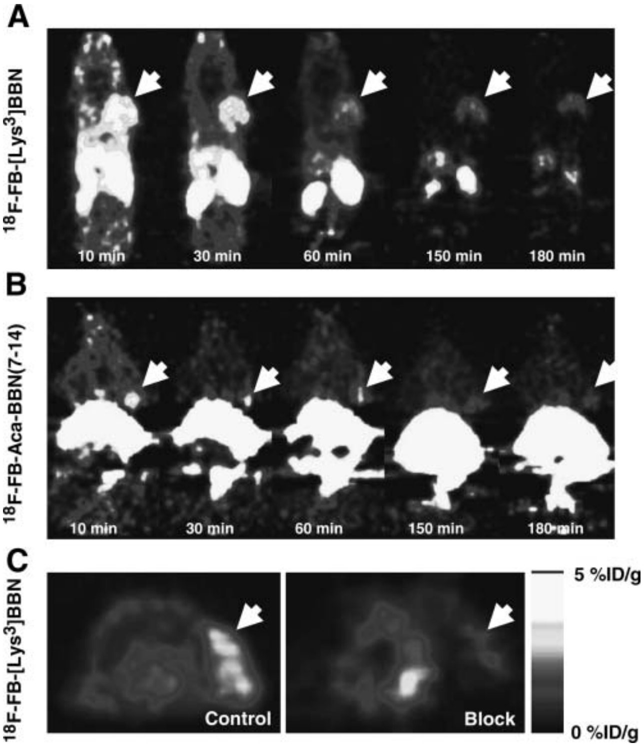

FIGURE 4. microPET images of athymic nude mice bearing PC-3 tumor on the right shoulder. Coronal images (decay corrected to time of tracer injection) were collected at multiple time points after injection of ^{18}F-FB-[Lys^{3}]BBN (A) or ^{18}F-FB-Aca-BBN(7–14) (B) (370 kBq/mouse). (C) Transaxial microPET images of PC-3 tumor-bearing mice at 1 h after tail vein injection of 3.7 MBq of ^{18}F-FB-[Lys^{3}]BBN in absence (Control) and presence (Block) of coinjected blocking dose of [Try^{4}]BBN (10 mg/kg mice body weight). Tumors are indicated by white arrows in all cases.

uptake of ^{18}F-FB-Aca-BBN(7–14) was 0.92, 0.71, and 0.78 %ID/g at 10, 30, and 60 min after injection, respectively. Liver had low uptake at all time points (1.35, 3.29, and 1.75 %ID/g at 5, 25, and 60 min after injection, respectively). The activity accumulation in the kidneys was also low at early time points (4.77 %ID/g at 5 min after injection) but increased to 11.19 %ID/g at 45 min after injection and remained steady over the remaining dynamic scan period. Figure 4C shows the transaxial microPET images of PC-3 tumor-bearing mice at 1 h after administration of ^{18}F-FB-[Lys^{3}]BBN, with and without coinjection of 10 mg/kg [Tyr^{4}]BBN. The blocking reduced the tumor uptake to 0.58 %ID/g at 1 h after injection, 4- to 5-fold lower than that of the control animals.

Metabolism of ^{18}F-FB-[Lys^{3}]BBN

The metabolic stability of ^{18}F-FB-[Lys^{3}]BBN was determined in mouse blood, urine, liver, kidney, and tumor homogenates at 60 min after injection The extraction efficiencies were 61.4% for the blood, 95.0% for the liver, 91.1% for the kidneys, and 97.8% for the PC-3 tumor, respectively. The elution efficiencies of the soluble fractions were 44.4% for the blood, 39.8% for the liver, 41.5% for the kidneys, and 95.5% for the PC-3 tumor. HPLC analysis results of the acetonitrile-eluted fractions are shown in Figure 6. The average fraction of intact tracer was between 0.7% and 47.2% (Table 1). Incubation of ^{18}F-FB-[Lys^{3}]BBN directly with tissue and organ homogenates revealed that the extraction efficiency was >90% in all cases, except for the liver, for which the extraction efficiency was only 67.7%. The elution efficiency was also >90% for all samples tested. Although we did not identify the composition of the metabolites, we found that all metabolites came off the HPLC column earlier than those for the parent compound. No defluoridation of ^{18}F-FB-[Lys^{3}]BBN was observed as no visible bone uptake was observed in any of the microPET scans.

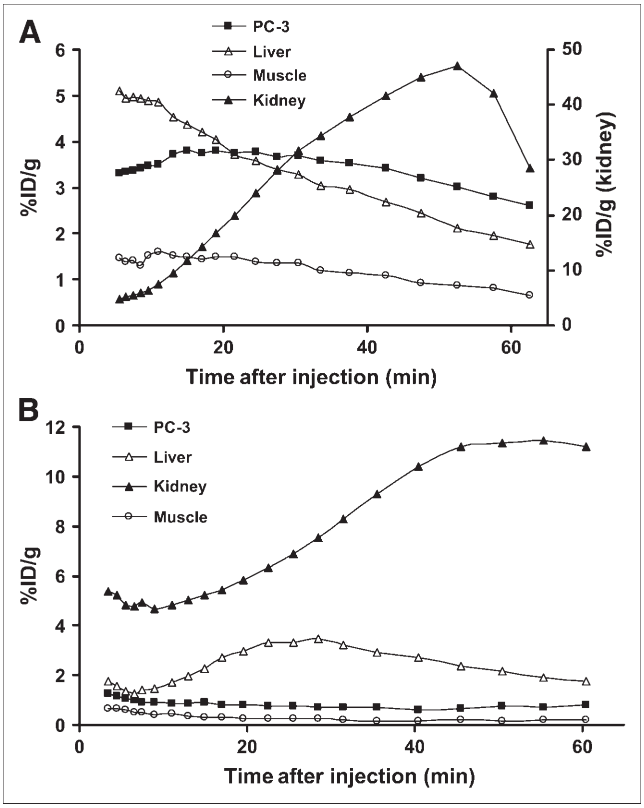

FIGURE 5. Time–activity curves of ^{18}F-FB-[Lys^{3}]BBN (A) and ^{18}F-FB-Aca-BBN(7–14) (B) derived from 60-min dynamic microPET scans. ROIs are shown for PC-3 tumor, liver, muscle, and kidney.

PET and CT Imaging of Orthotopic PC-3 Tumor Model

We also evaluated ^{18}F-FB-[Lys^{3}]BBN in orthotopic PC-3 tumor-bearing mice. The representative microPET images shown in Figure 7A were at 17 min after injection The orthotopic tumor uptake was calculated to be 2.07 %ID/g from microPET imaging, which is somewhat lower than that of subcutaneous PC-3 tumor (3.74 %ID/g at 17 min after injection). Dynamic scans indicated that the tumor was clearly visualized between 10 and 30 min, after which a significant amount of urinary bladder activity interferes

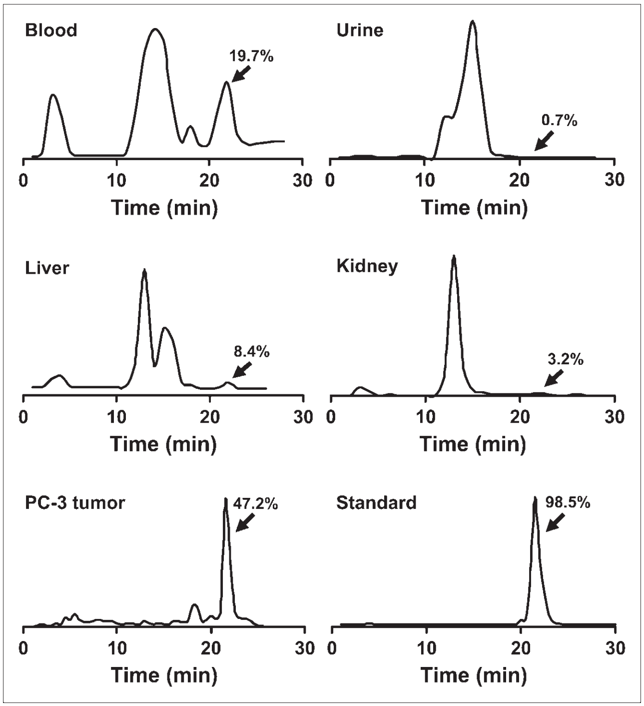

FIGURE 6. HPLC profiles of soluble fractions of blood, urine, liver, kidney, and tumor homogenates collected at 1 h after injection of ^{18}F-FB-[Lys^3]BBN to a male athymic PC-3 tumor-bearing nude mouse. As a comparison, the HPLC profile of intact tracer (Standard) is also shown.

with the tumor delineation. The presence of the well-established tumor grown in the prostate gland was confirmed by microCT without a contrast agent (Fig. 7A). Good visual agreement after registration was obtained in all sagittal, coronal, and transaxial images (Fig. 7A). The registration is focused on the tumor region and did not use markers that can be shifted or displaced. The whole registration procedure took <15 min on a standard personal computer, as the narrow-band approach used is a compact representation of a structure where only pixels close to the structure boundaries are considered (*30*). Both subcutaneous and orthotopic PC-3 tumor tissues were also resected for histology to verify the characterization of tumors ex vivo. The hematoxylin–eosin staining results (Fig. 7B) of both PC-3 tumors showed similar morphology characteristic of cancer cells.

DISCUSSION

There has been an exponential growth in the development of radiolabeled peptides for diagnostic and therapeutic applications in the last decade. Peptidic radiopharmaceuticals have many favorable properties, including fast clearance, rapid tissue penetration, and low antigenecity, and can be produced easily and inexpensively (*31*). However, there may be problems with the in vivo catabolism, unwanted physiologic effects, and chelate attachment. Most studies have been focused on radiometal labeling of peptides for SPECT imaging of receptors that are overexpressed on the diseased cells (*32–34*). More recently, peptides have been conjugated to macrocyclic chelators for labeling of ^{64}Cu, ^{86}Y, and ^{68}Ga for PET applications (*17,20,35,36*). Because of the overexpression of GRPR in a variety of cancers, bombesin analogs—derived either from the full tetradecapeptide sequence or from a truncated C-terminal portion of the peptide—have been labeled with various radiometals

TABLE 1
Extraction Efficiency and Elution Efficiency Data and HPLC Analysis of Soluble Fraction of Tissue Samples at 60 Minutes After Injection

	Extraction efficiency[*] (%)				
Fraction	Blood	Urine	Liver	Kidney	PC-3
Unsoluble fraction[†]	38.6 (2.0)	ND	5.0 (32.3)	8.9 (6.8)	2.2 (0.3)
Soluble fraction[‡]	61.4 (98.0)	ND	95.0 (67.7)	91.1 (93.2)	97.8 (99.7)
	Elution efficiency (%)				
Nonretained fraction[§]	52.5 (7.9)	ND	55.3 (2.4)	57.1 (1.4)	2.9 (1.7)
Wash water[‖]	3.2 (1.8)	ND	4.9 (1.8)	1.4 (1.3)	1.7 (0.6)
Acetonitrile eluent[¶]	44.4 (90.3)	ND	39.8 (95.8)	41.5 (97.3)	95.5 (97.7)
	HPLC analysis (%)				
Intact tracer	19.7	0.7	8.4	3.2	47.2

---

[*] Results in parentheses are from direct mixing of ^{18}F-FB-[Lys^3]BBN with tissue homogenates.
[†] Amount of activity retained in pellets.
[‡] Amount of activity that was extracted to PBS solution.
[§] Amount of activity that could not be trapped onto C_{18} cartridge.
[‖] Amount of activity that was eluted from C_{18} cartridge using 2 mL of water.
[¶] Amount of activity that was eluted from C_{18} cartridge using 2 mL of acetonitrile with 0.1% TFA.
ND = not determined.

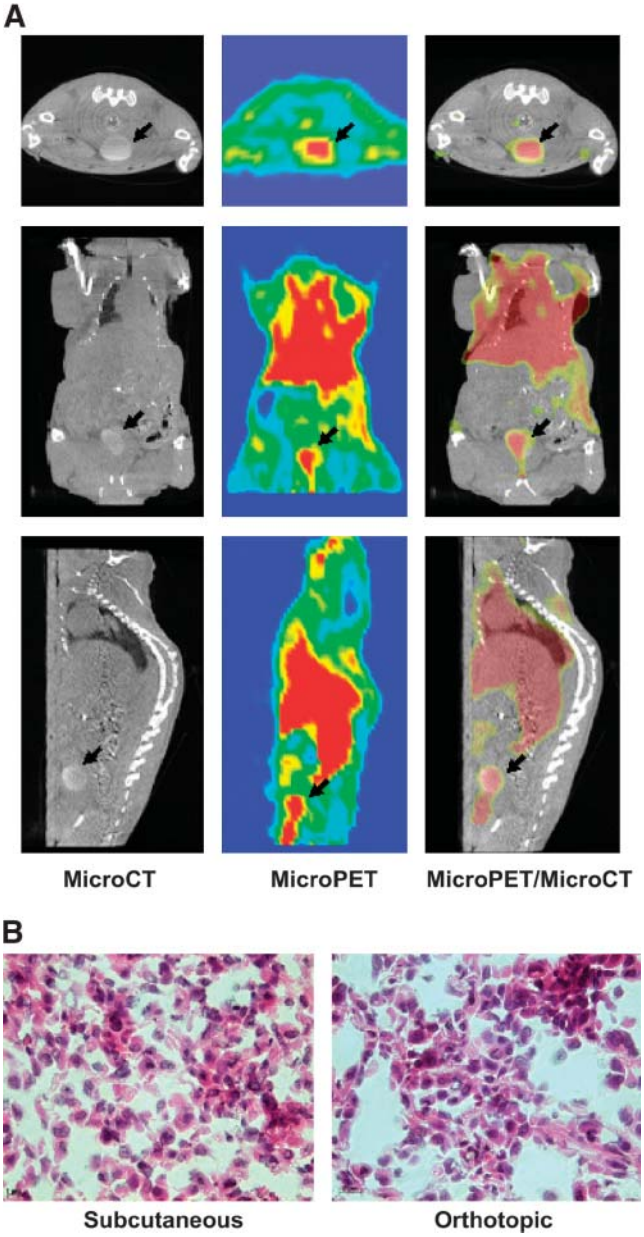

FIGURE 7. (A) microPET and microCT visualization of orthotopic PC-3 tumor. Representative transverse, coronal, and sagittal images that contain the tumor at 17 min after injection of 3.7 MBq of ^{18}F-FB-[Lys^3]BBN are shown. The tumor grown in mouse prostate gland is confirmed by microCT scan without contrast agent. Coregistration of microPET (slice thickness, 1.2 mm) and microCT (slice thickness, 80 μm) is accomplished by using a narrow-band approach without the need for fiducial markers. (B) Hematoxylin–eosin staining (×400) of subcutaneous (left) and orthotopic (right) PC-3 tumor tissues.

for both PET (^{64}Cu and ^{68}Ga) and SPECT (^{99m}Tc and ^{111}In) imaging applications (*14,15,17,18,20,37*). ^{18}F is an ideal short-lived PET isotope for labeling small molecular recognition units, such as biologically active peptides, and it is easily produced in the small biomedical cyclotrons. Most peptides have the N-terminal primary amine group and one or more lysine ε-amino residues that can be labeled with ^{18}F through an amine-reactive prosthetic labeling group such as ^{18}F-SFB (*22*). Thus, we decided to label both peptides ([Lys^3]BBN and Aca-BBN(7–14)) with ^{18}F for in vitro and in vivo characterizations.

Our cell-binding assay experiment demonstrated that the truncated peptide sequence Aca-BBN(7–14) had significantly lower receptor-binding affinity than that of [Lys^3]BBN. ^{18}F-labeled Aca-BBN(7–14) was also less potent than the corresponding bombesin peptide analogs. Both tracers are metabolically unstable after intravenous administration. Multiple metabolites were found but not characterized here. Identification of the composition of the degradation products may be important to identify the cleavage sites to design and characterize peptides of enhanced metabolic stability.

The internalization and efflux patterns of ^{18}F-FB-[Lys^3]BBN and ^{18}F-FB-Aca-BBN(7–14) are of note. ^{18}F-FB-[Lys^3]BBN with higher receptor affinity than ^{18}F-FB-Aca-BBN(7–14) showed significantly higher cellular uptake. Both tracers, however, had a rapid washout after reaching a maximum at 15 min of incubation with PC-3 cells (Fig. 2A), which is similar to ^{125}I-[Tyr^4]BBN but very different from radiometal-labeled BBNs. The prolonged retention of ^{99m}Tc-, ^{111}In-, or ^{64}Cu-labeled BBNs is most likely due to the lack of cell permeability of the hydrophilic macrocyclic conjugate (*14,15,17*). In the case of ^{18}F-labeled bombesin analogs, after GRPR-mediated internalization, both the intact tracer and the metabolized peptide fractions that are radioactive remain to be lipophilic and, thus, more amenable to penetration in and out of the cells. It is, thus, not surprising to observe rapid externalization of both ^{18}F-FB-[Lys^3]BBN and ^{18}F-FB-Aca-BBN(7–14), with the less-potent ^{18}F-FB-Aca-BBN(7–14) effluxed even more rapidly than ^{18}F-FB-[Lys^3]BBN (Fig. 2B). Such in vitro characters of ^{18}F-labeled bombesin analogs tally with the relatively short half-life of ^{18}F.

^{18}F-FB-[Lys^3]BBN with higher receptor affinity and prolonged cell retention than ^{18}F-FB-Aca-BBN(7–14) also exhibited superior tumor-targeting efficacy and pharmacokinetics in vivo. Although ^{18}F-FB-Aca-BBN(7–14) showed some contrast at early time points, the activity accumulation in the tumor was quickly washed out. Because of the lipophilic character of ^{18}F-FB-Aca-BBN(7–14), it exhibited both hepatobiliary and renal clearance routes as evidenced by very strong signal in the liver, gallbladder, and lower abdomen, eliminating the potential of this compound for detecting the orthotopic prostate cancer that is located very close to the urinary bladder. A strong tumor-to-background contrast was observed for ^{18}F-FB-[Lys^3]BBN in PC-3 tumor, although the magnitude of tracer uptake is significantly lower than that obtained from biodistribution studies. A similar phenomenon has been observed for ^{64}Cu-DOTA-[Lys^3]BBN (*19*). We reason that the amount of tracer administered for PET is about an order of magnitude higher than that for biodistribution, which may have caused partial self-inhibition of receptor-specific uptake in PC-3 tumor. We also noticed that nonradioactive BBN is able to effectively inhibit the tumor uptake of ^{18}F-FB-[Lys^3]BBN despite of the relatively low metabolic stability of the tracer. The substantial blockade of tumor uptake by unlabeled BBN suggests that some of the degraded radioactive components accumulated in the tumor may also have affinity for GRP receptor, which can be replaced by BBN.

microPET/microCT coregistration using ^{18}F-FB-[Lys^3]BBN is a powerful tool for orthotopic prostate cancer imaging. The high-resolution microCT scan provides good contrast for PC-3 tumor without the need of contrast-enhancing media, whereas microPET imaging with ^{18}F-FB-[Lys^3]BBN offers the GRPR expression level of the tumor. In general, image registration can be formulated as an optimization problem where the variables are a group of transformation parameters that lead to the best match between the input images. The match is quantified in mathematic terms by the use of a metric, which ranks a potential matching based on the image histograms, resolution, or pixel values of the involved organs. Usage of MI has been widely adopted when dealing with multimodality image registration (*38*). However, MI cannot be applied directly to PET/CT registration for soft tissue because the wide pixel intensities within an organ as imaged in the PET images produce multiple correspondences with the CT images that act as noise to the registration algorithm, hindering its convergence (*39*). Therefore, only marker-based techniques have been reported for PET/CT registration of mice studies (*40*). The narrow-band approach used in this study was originally devised for magnetic resonance spectroscopic imaging (MRSI)/CT registration, where a similar noncorrelation of pixel intensities was observed (*30*). Previous studies have suggested that this 2-step image registration technique improves the convergence behavior of the calculation and reduces the computational efforts because sophisticated statistical considerations can be replaced with simpler pixel-based metrics computed only in the regions of clinical interest.

CONCLUSION

This study demonstrated the successful coupling of [Lys^3]BBN and Aca-BBN(7–14) with positron-emitting radionuclide ^{18}F through the prosthetic labeling group ^{18}F-SFB. The bombesin analog with the full tetradecapeptide sequence (^{18}F-FB-[Lys^3]BBN) is superior to that with a truncated C-terminal sequence (^{18}F-FB-Aca-BBN(7–14)) in terms of GRPR avidity, receptor-mediated internalization rate, intracellular retention, tumor-targeting efficacy, and in vivo pharmacokinetics. Although ^{18}F-FB-[Lys^3]BBN is relatively metabolically unstable, dynamic PET scans demonstrated the ability of this tracer to visualize both subcutaneous and orthotopic PC-3 tumor in murine xenograft models. Furthermore, ^{18}F-FB-[Lys^3]BBN may also be used for localization of other tumors that are GRPR positive.

ACKNOWLEDGMENTS

This work was supported, in part, by Department of Defense (DOD) Prostate Cancer Research Program (PCRP) New Investigator Award (NIA) DAMD1717-03-1-0143, National Cancer Institute (NCI) grant R21 CA102123, National Institute of Biomedical Imaging and Bioengineering (NIBIB) grant R21 EB001785, DOD Breast Cancer Research Program (BCRP) Concept Award DAMD17-03-1-0752, DOD BCRP IDEA Award W81XWH-04-1-0697, American Lung Association California, Society of Nuclear Medicine Education and Research Foundation, NCI Small Animal Imaging Resource Program (SAIRP) grant R24 CA93862, and NCI In Vivo Cellular Molecular Imaging Center (ICMIC) grant P50 CA114747. Dr. Zhengming Xiong is acknowledged for cell culture and the authors thank Pauline Chu for histology.

REFERENCES

1. di Sant'Agnese PA. Neuroendocrine cells of the prostate and neuroendocrine differentiation in prostatic carcinoma: a review of morphologic aspects. *Urology.* 1998;51:121–124.
2. Vashchenko N, Abrahamsson PA. Neuroendocrine differentiation in prostate cancer: implications for new treatment modalities. *Eur Urol.* 2005;47:147–155.
3. Chung DH, Evers BM, Beauchamp RD, et al. Bombesin stimulates growth of human gastrinoma. *Surgery.* 1992;112:1059–1065.
4. Glover SC, Tretiakova MS, Carroll RE, Benya RV. Increased frequency of gastrin-releasing peptide receptor gene mutations during colon-adenocarcinoma progression. *Mol Carcinog.* 2003;37:5–15.
5. Battey J, Wada E, Corjay M, et al. Molecular genetic analysis of two distinct receptors for mammalian bombesin-like peptides. *J Natl Cancer Inst Monogr.* 1992;13:141–144.
6. Scheffel U, Pomper MG. PET imaging of GRP receptor expression in prostate cancer. *J Nucl Med.* 2004;45:1277–1278.
7. Matusiak D, Glover S, Nathaniel R, Matkowskyj K, Yang J, Benya RV. Neuromedin B and its receptor are mitogens in both normal and malignant epithelial cells lining the colon. *Am J Physiol Gastrointest Liver Physiol.* 2005; 288:G718–G728.
8. Fathi Z, Corjay MH, Shapira H, et al. BRS-3: a novel bombesin receptor subtype selectively expressed in testis and lung carcinoma cells. *J Biol Chem.* 1993; 268:5979–5984.
9. Pinski J, Reile H, Halmos G, Groot K, Schally AV. Inhibitory effects of somatostatin analogue RC-160 and bombesin/gastrin-releasing peptide antagonist RC-3095 on the growth of the androgen-independent Dunning R-3327-AT-1 rat prostate cancer. *Cancer Res.* 1994;54:169–174.
10. Reubi JC, Macke HR, Krenning EP. Candidates for peptide receptor radiotherapy today and in the future. *J Nucl Med.* 2005;46(suppl 1):67S–75S.
11. Maina T, Nock BA, Zhang H, et al. Species differences of bombesin analog interactions with GRP-R define the choice of animal models in the development of GRP-R-targeting drugs. *J Nucl Med.* 2005;46:823–830.
12. Varvarigou A, Bouziotis P, Zikos C, Scopinaro F, De Vincentis G. Gastrin-releasing peptide (GRP) analogues for cancer imaging. *Cancer Biother Radiopharm.* 2004;19:219–229.
13. Van de Wiele C, Dumont F, Dierckx RA, et al. Biodistribution and dosimetry of ^{99m}Tc-RP527, a gastrin-releasing peptide (GRP) agonist for the visualization of GRP receptor-expressing malignancies. *J Nucl Med.* 2001;42:1722–1727.
14. Scopinaro F, De Vincentis G, Corazziari E, et al. Detection of colon cancer with ^{99m}Tc-labeled bombesin derivative (^{99m}Tc-Leu^{13}-BN1). *Cancer Biother Radiopharm.* 2004;19:245–252.
15. Zhang H, Chen J, Waldherr C, et al. Synthesis and evaluation of bombesin derivatives on the basis of pan-bombesin peptides labeled with indium-111, lutetium-177, and yttrium-90 for targeting bombesin receptor-expressing tumors. *Cancer Res.* 2004;64:6707–6715.
16. Smith CJ, Sieckman GL, Owen NK, et al. Radiochemical investigations of [^{188}Re(H$_2$O)(CO)$_3$-diaminopropionic acid-SSS-bombesin(7-14)NH$_2$]: syntheses, radiolabeling and in vitro/in vivo GRP receptor targeting studies. *Anticancer Res.* 2003;23:63–70.
17. Rogers BE, Bigott HM, McCarthy DW, et al. MicroPET imaging of a gastrin-releasing peptide receptor-positive tumor in a mouse model of human prostate cancer using a ^{64}Cu-labeled bombesin analogue. *Bioconjug Chem.* 2003;14: 756–763.

18. Rogers BE, Manna DD, Safavy A. In vitro and in vivo evaluation of a ^{64}Cu-labeled polyethylene glycol-bombesin conjugate. *Cancer Biother Radiopharm.* 2004;19:25–34.
19. Chen X, Park R, Hou Y, et al. MicroPET and autoradiographic imaging of GRP receptor expression with ^{64}Cu-DOTA-[Lys^3]bombesin in human prostate adenocarcinoma xenografts. *J Nucl Med.* 2004;45:1390–1397.
20. Schuhmacher J, Zhang H, Doll J, et al. GRP receptor-targeted PET of a rat pancreas carcinoma xenograft in nude mice with a ^{68}Ga-labeled bombesin(6-14) analog. *J Nucl Med.* 2005;46:691–699.
21. Okarvi SM. Recent progress in fluorine-18 labelled peptide radiopharmaceuticals. *Eur J Nucl Med.* 2001;28:929–938.
22. Vaidyanathan G, Zalutsky MR. Improved synthesis of N-succinimidyl 4-[^{18}F]fluorobenzoate and its application to the labeling of a monoclonal antibody fragment. *Bioconjug Chem.* 1994;5:352–356.
23. Chen X, Park R, Shahinian AH, et al. ^{18}F-Labeled RGD peptide: initial evaluation for imaging brain tumor angiogenesis. *Nucl Med Biol.* 2004;31:179–189.
24. Wu Y, Zhang X, Xiong Z, et al. MicroPET imaging of glioma α_v-integrin expression using ^{64}Cu-labeled tetrameric RGD peptide. *J Nucl Med.* 2005;46:1707–1718.
25. Chen X, Park R, Hou Y, et al. MicroPET imaging of brain tumor angiogenesis with ^{18}F-labeled PEGylated RGD peptide. *Eur J Nucl Med Mol Imaging.* 2004; 31:1081–1089.
26. Chen X, Tohme M, Park R, Hou Y, Bading JR, Conti PS. Micro-PET imaging of $\alpha_v\beta_3$-integrin expression with ^{18}F-labeled dimeric RGD peptide. *Mol Imaging.* 2004;3:96–104.
27. Chen X, Park R, Tohme M, Shahinian AH, Bading JR, Conti PS. MicroPET and autoradiographic imaging of breast cancer α_v-integrin expression using ^{18}F- and ^{64}Cu-labeled RGD peptide. *Bioconjug Chem.* 2004;15:41–49.
28. Hillman GG, Wang Y, Kucuk O, et al. Genistein potentiates inhibition of tumor growth by radiation in a prostate cancer orthotopic model. *Mol Cancer Ther.* 2004;3:1271–1279.
29. Boellaard R, van Lingen A, Lammertsma AA. Experimental and clinical evaluation of iterative reconstruction (OSEM) in dynamic PET: quantitative characteristics and effects on kinetic modeling. *J Nucl Med.* 2001;42:808–817.
30. Schreibmann E, Xing L. Narrow band deformable registration of prostate magnetic resonance imaging, magnetic resonance spectroscopic imaging, and computed tomography studies. *Int J Radiat Oncol Biol Phys.* 2005;62:595–605.
31. Benedetti E, Morelli G, Accardo A, Mansi R, Tesauro D, Aloj L. Criteria for the design and biological characterization of radiolabeled peptide-based pharmaceuticals. *BioDrugs.* 2004;18:279–295.
32. Nock BA, Nikolopoulou A, Galanis A, et al. Potent bombesin-like peptides for GRP-receptor targeting of tumors with ^{99m}Tc: a preclinical study. *J Med Chem.* 2005;48:100–110.
33. Janssen ML, Oyen WJ, Dijkgraaf I, et al. Tumor targeting with radiolabeled $\alpha_v\beta_3$ integrin binding peptides in a nude mouse model. *Cancer Res.* 2002;62:6146–6151.
34. De Jong M, Valkema R, Van Gameren A, et al. Inhomogeneous localization of radioactivity in the human kidney after injection of [^{111}In-DTPA]octreotide. *J Nucl Med.* 2004;45:1168–1171.
35. Chen X, Liu S, Hou Y, et al. MicroPET imaging of breast cancer α_v-integrin expression with ^{64}Cu-labeled dimeric RGD peptides. *Mol Imaging Biol.* 2004; 6:350–359.
36. Chen X, Sievers E, Hou Y, et al. Integrin $\alpha_v\beta_3$-targeted imaging of lung cancer. *Neoplasia.* 2005;7:271–279.
37. Hoffman TJ, Gali H, Smith CJ, et al. Novel series of ^{111}In-labeled bombesin analogs as potential radiopharmaceuticals for specific targeting of gastrin-releasing peptide receptors expressed on human prostate cancer cells. *J Nucl Med.* 2003;44:823–831.
38. Maes F, Collignon A, Vandermeulen D, Marchal G, Suetens P. Multimodality image registration by maximization of mutual information. *IEEE Trans Med Imaging.* 1997;16:187–198.
39. du Bois d'Aische A, Craene MD, Geets X, Gregoire V, Macq B, Warfield SK. Efficient multi-modal dense field non-rigid registration: alignment of histological and section images. *Med Image Anal.* 2005;9:538–546.
40. Thomas CT, Meyer CR, Koeppe RA, et al. A positron-emitting internal marker for identification of normal tissue by positron emission tomography: phantom studies and validation in patients. *Mol Imaging Biol.* 2003;5:79–85.